Biomedicine & Pharmacotherapy 169 (2023) 115940

Contents lists available at ScienceDirect

Biomedicine & Pharmacotherapy

journal homepage: www.elsevier.com/locate/biopha

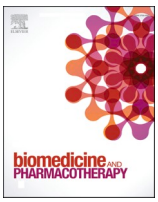

Inhibition of furin-like enzymatic activities and SARS-CoV-2 infection by osthole and phenolic compounds with aryl side chains

Yuka Kiba [a,1], Takashi Tanikawa [a,*,1], Tsuyoshi Hayashi [b,1], Hitoshi Kamauchi [c,1], Taishi Seki [a], Ryuichiro Suzuki [c], Masashi Kitamura [a,*]

[a] School of Pharmacy, Faculty of Pharmacy and Pharmaceutical Sciences, Josai University; 1–1, Keyakidai, Sakado, Saitama 350–0295, Japan
[b] Department of Virology II, National Institute of Infectious Diseases, Tokyo, Japan
[c] Department of Pharmaceutical Sciences, Faculty of Pharmacy and Pharmaceutical Sciences, Josai University, 1-1 Keyakidai, Sakado City, Saitama 350-0295, Japan

ARTICLE INFO

Keywords:
Furin
SARS-CoV-2
Osthole
Coumarin

ABSTRACT

Coronavirus disease 2019 (COVID-19), caused by severe acute respiratory syndrome coronavirus 2 (SARS-CoV-2), spread as a pandemic and caused damage to people's lives and countries' economies. The spike (S) protein of SARS-CoV-2 contains a cleavage motif, Arg-X-X-Arg, for furin and furin-like enzymes at the boundary of the S1/S2 subunits. Given that cleavage plays a crucial role in S protein activation and viral entry, the cleavage motif was selected as the target. Our previous fluorogenic substrate study showed that osthole, a coumarin compound, inhibits furin-like enzyme activity. In this study, we examined the potential activities of 15 compounds with a structure-activity relationship with osthole, and evaluated their protective ability against SARS-CoV-2 infection. Of the 15 compounds tested, compounds **C1** and **C2** exhibited the inhibitory effects of osthole against furin-like enzymatic activity; however, little or no inhibitory effects against furin activity were observed. We further examined the inhibition of SARS-CoV-2 activity by compounds **C1** and **C2** using a Vero E6 cell line that expresses the transmembrane protease serine 2 (TMPRSS2). Compounds **C1**, **C2**, and osthole effectively inhibited SARS-CoV-2 infection. Therefore, osthole and its derivatives can potentially be used as therapeutic agents against SARS-CoV-2.

1. Introduction

Severe acute respiratory syndrome coronavirus 2 (SARS-CoV-2) was discovered in Wuhan, China in December 2019 and rapidly spread worldwide [1]. Coronavirus disease 2019 (COVID-19) caused by SARS-CoV-2 has typical clinical symptoms such as fever, cough, breathing difficulties, and pneumonia and may result in acute respiratory distress syndrome [2]. As of September 2023, more than 770,000,000 confirmed cases of COVID-19, with more than 6900,000 deaths, have been reported worldwide [3]. Several highly effective vaccines against SARS-CoV-2 have been approved and are currently used in various countries [4]. Vaccination against SARS-CoV-2 is important; however, new variants of SARS-CoV-2 are emerging, and the effects of these vaccines remain unclear [5]. Therefore, antiviral drugs as complements to vaccines are required to reduce the global burden of this pandemic. SARS-CoV-2 is a single-stranded positive-sense RNA virus that enters cells by binding to the angiotensin-converting enzyme 2 (ACE2) receptor [6,7]. The entry of SARS-CoV-2 into host cells is mediated by the interaction of the spike (S) protein with the ACE2 receptor on the host cells. SARS-CoV-2 entry requires cleavage of the S protein by the host cell transmembrane protease serine 2 (TMPRSS2)[7]. Cells infected with SARS-CoV-2 fuse with adjacent ACE2-expressing cells to form morphologically distinct multinuclear giant cells (syncytia) [8,9]. Spike-mediated syncytia have been reported in lung samples from COVID-19 patients [10,11].

The S protein on the viral surface is cleaved into the S1 and S2 subunits. The S1 subunit contains a receptor-binding domain (RBD) that binds ACE2 to host cells and the S2 subunit has a fusion peptide (FP) domain that mediates membrane fusion. The proteolytic cleavage of the viral envelope is required for viral entry[12]. Furin, a

Abbreviations: SARS-CoV-2, severe acute respiratory syndrome coronavirus 2; ACE2, angiotensin-converting enzyme 2; TMPRSS2, Transmembrane protease serine 2; RBD, receptor-binding domain; FCS, furin cleavage site; PCs, proprotein convertases; TGF-β1, transforming growth factor-beta1.

* Corresponding authors.
E-mail addresses: tanikawa@josai.ac.jp (T. Tanikawa), kitamura@josai.ac.jp (M. Kitamura).

[1] These authors contributed equally to this study

https://doi.org/10.1016/j.biopha.2023.115940
Received 11 September 2023; Received in revised form 21 November 2023; Accepted 21 November 2023
Available online 25 November 2023

calcium-dependent serine endoprotease widely present in human cells, cleaves the S protein at the S1/S2 boundary site. Cleavage plays a crucial role in protein activation and viral entry [12]. Unlike SARS-CoV, the S protein of SARS-CoV-2 has a furin cleavage site (FCS) of four critical amino acids, Arg-Arg-Ala-Arg (RRAR), for furin and furin-like enzymes at the S1/S2 cleavage site, matching the consensus amino acid motif of the substrate for furin and other proprotein convertases (PCs) [12,13]. Cleavage at the FCS is related to the processing and activation of endogenous proproteins, including transforming growth factor (TGF)-β1 and viral membrane proteins such as HIV glycoprotein gp160 and highly pathogenic avian influenza of hemagglutinin[14–16]. Furin inhibitors block the SARS-CoV-2 S protein cleavage to suppress viral entry [9,12,13]. In addition, mutation of the FCS in the SARS-CoV-2 S protein efficiently reduces its entry into host cells [12,13]. The pathogenesis of mutant SARS-CoV-2 with FCS deletion is attenuated in hamsters, K18-hACE2 transgenic mice, and ferrets during the pathogenesis of SARS-CoV-2 [17,18]. Therefore, inhibitory molecules of furin have great therapeutic potential for overcoming COVID-19.

We previously screened 124 crude herbal drugs for their inhibitory effects on furin-like activity based on a fluorogenic furin-like assay; *Cnidium monnieri* fruit and its component, osthole, inhibited furin-like activity [19]. We also reported that honokiol suppresses furin-like enzymatic activity and can potentially inhibit SARS-CoV-2 infection [20]. Both osthole and honokiol contained phenoxy groups and aryl side chains. This structure is essential for the inhibitory effects. Therefore, we hypothesized that a compound with strong inhibitory effects on furin-like activity would effectively suppress SARS-CoV-2 infection. In this study, we designed and synthesized coumarin derivatives containing a phenoxy group with an aryl side chain as the core structure to target furin-like enzymatic activity. We evaluated their protective ability against SARS-CoV-2 infection.

2. Materials and methods

2.1. Compound synthesis

2.1.1. Materials for compound synthesis

C11 (2′,4′, 6′-trihydroxy acetophenone monohydrate, Tokyo Chemical Industry Co., Ltd., Tokyo, Japan), **C12** (2,4-dihydroxy-6-methylbenzaldehyde, FUJIFILM Wako Pure Chemical Co., Osaka, Japan), **C13** (Umbelliferone, Sigma-Aldrich, MO, USA), **C14** (2′,4′-dihydroxyacetophenone, Tokyo Chemical Industry Co.), and osthole (Tokyo Chemical Industry Co.) were obtained from commercial suppliers.

2.1.2. Preparation of C1–C8

Solutions of **C11**, **C12**, **C13,** or **C14** (1 equiv.) in acetone (10.0 mL) and K_2CO_3 (2 equiv.) were reacted with 3,3-dimethylallyl bromide or geranyl bromide (1 equiv.). The mixture was stirred for one hour and then extracted with ethyl acetate (EtOAc) and H_2O. The organic layer was dried using Na_2SO_4 and purified by silica gel column chromatography (*n*-hexane: EtOAc) to yield the corresponding *O*-alkyl ethers (yields: **C1** 30%, **C2** 32%, **C3** 75%, **C4** 63%, **C5** 44%, **C6** 40%, **C7** 10%, and **C8** 13%). The structures of known compounds (**C1**, **C2**, **C5**, **C6**, **C7**, **C8**) were identified by comparing their NMR spectra [21–25]. The structures of **C3** and **C4** were determined using ^{1}H NMR (400 MHz) and ^{13}C NMR (100 MHz) (Fig. S1).

2.1.3. Preparation of C9 and C10

A solution of osthole (60.0 mg; 0.25 mmol) and palladium 10% on carbon (25.0 mg) in ethanol (10.0 mL) was stirred under hydrogen for 12 h at room temperature. The reaction mixture was filtered through a cerite filter and concentrated. The crude mixture was purified by silica-gel column chromatography (*n*-hexane-EtOAc 10:1) to obtain compounds **C9** (10.0 mg 0.034 mmol, 14%) and **C10** (31.5 mg, 0.13 mmol, 52%). The structures of **C9** and **C10** were determined using ^{1}H NMR (400 MHz) and ^{13}C NMR (100 MHz) (Fig. S1). All reagents and solvents were purchased from commercial suppliers and used without further purification. 1D and 2D NMR spectra were measured at 298 K with a Bruker Avance NEO 400 MHz spectrometer (Bruker Japan K.K., Kanagawa, Japan) using tetramethylsilane as the internal standard. Column chromatography was performed using a Wakogel C-200 column (FUJIFILM Wako Pure Chemical Corporation).

2.2. Furin-like and furin activity based on fluorogenic substrate

A furin-like enzymatic assay based on fluorogenic substrates was conducted as previously described, with minor modifications [19,20]. Fluorogenic substrates (pyr-Arg-Arg-Ala-Arg-MCA) were obtained from Greiner Bio-One (Austria). Caco-2 cells (RCB0988; RIKEN BioResource Center, Tsukuba, Japan) were maintained in Eagle's minimum essential medium (EMEM) supplemented with 20% fetal bovine serum, 2 mmol/L L-glutamine, 100 μg/mL streptomycin, and 100 units/mL penicillin. The cells were lysed with assay buffer (20 mM HEPES-KOH (pH 7.4)) and 1 mM $CaCl_2$ containing 0.1% Triton X-100) and used as furin-like enzymes in the whole-cell lysate. The whole-cell lysate was diluted based on the cleavage activity equivalent to 100 U furin (R&D Systems, Minneapolis, MN, USA) and used for the enzymatic assay.

Secreted soluble human furin (ssfurin) was expressed and purified as described previously[26]. Human furin (accession No. NM_001289823) was synthesized by Vector Builder, Inc. (IL, USA). The ssfurin (aa. 1–704), which lacked the C-terminal domain, with a His × 6 tag at the C-terminus, was cloned into pcDNA3.1, using In-Fusion cloning (Takara Bio, Shiga, Japan). Plasmids were transfected into HEK293 cells (JCRB9068; JCRB Cell Bank, Osaka, Japan) using TransIT293 reagent (Takara). The transfected cells were maintained in Dulbecco's modified Eagle's medium (DMEM) containing 10% FBS and selected by the addition of G418 (750 μg/mL) in the culture medium. The culture medium was replaced with serum-free DMEM and the cells were incubated for 12 h. After incubation, the culture medium was collected and purified by ultrafiltration (10 kDa NMWL; Millipore, Molsheim, France). The ultrafiltration fraction (> 10 kDa) was collected by adding the assay buffer and used for the furin enzyme assay. Ssfurin was separated on a 12% SDS-PAGE gel and analyzed using western blotting (Fig. S2). The collected furin was diluted based on cleavage activity equivalent to 15 U of commercial furin (R&D Systems, Inc.) activity.

Furin-like and furin assays were performed by adding enzyme solution, assay buffer, and sample or control buffer to each well of a 96-well black plate. After incubation at 37 °C for 30 min, 100 μM pyr-Arg-Arg-Ala-Arg-MCA were added to each well, and after further incubation for 60 min, the enzyme activity was determined by measuring the fluorescence intensity of 7-amino-4-methyl coumarin (AMC) (ex. 380 nm /em. 460 nm) using a Synergy H1 (Agilent Technologies, Santa Clara, CA, USA). Dec-RVKR-CMK (Cayman Chemical, MI, USA) was used as a positive control.

2.3. SARS-CoV-2 infection

Vero E6 cells overexpressing TMPRSS2 protein (Vero E6/TMPRSS2, JCRB1819, JCRB Cell Bank, Osaka, Japan) were cultured in DMEM supplemented with 10% FBS, 100 U/mL penicillin, 100 μg/mL streptomycin, and 1 mg/mL G418 (Nacalai Tesque) [20]. Cell viability in Vero E6/TMPRSS2 cells upon compound treatment was determined using CellTiter-Glo® Luminescent Cell Viability Assay (Promega, Madison, WI, USA). The SARS-CoV-2 infection studies were performed as previously described [20]. Briefly, confluent Vero E6/TMPRSS2 cells cultured in a 96-well plate (CellCarrier-96 Ultra, Perkin Elmer, Waltham, MA, USA) were infected with 2019-nCoV/Japan/-TY/WK-521/2020 strain (WK-521) of SARS-CoV-2 at a multiplicity of infection (MOI) of 0.009 in the presence of the compounds at the indicated concentrations for 24 hr at 37 °C [27]. The infected cells were fixed with 4% paraformaldehyde in D-PBS for 30 min and permeabilized with 0.2% Triton X-100 in D-PBS for 15 min. The cells were stained for

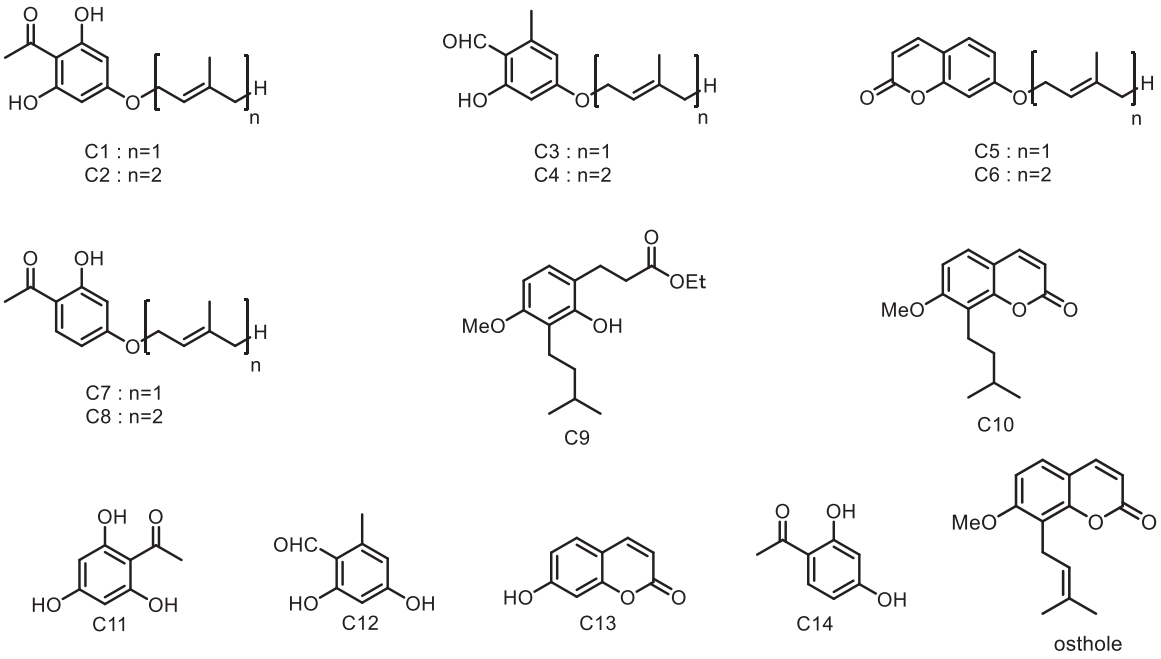

Fig. 1. Preparation of coumarin derivatives.

SARS-CoV-2 S protein using rabbit anti-SARS-CoV-2 Spike RBD monoclonal antibody (1:3000, clone HL1003, GTX635792; GeneTex, Irvine, CA, USA), followed by goat anti-rabbit IgG Alexa Fluor 488 (1:1000; Life Technologies, Carlsbad, CA, USA). Cell nuclei were stained with 1 μg/mL 4,6-diamidino-2-phenylindole (DAPI) solution (Dojindo Laboratories, Kumamoto, Japan). The cells were then imaged using the Operetta CLS High-Content Analysis System (Perkin Elmer), and infectivity (percentage of SARS-CoV-2 positive cells) in each well was calculated by counting SARS-CoV-2 S-and DAPI-positive cells using Harmony software (Perkin Elmer). A dose-response curve was created using a nonlinear regression model, and the half-maximal inhibitory concentration (IC_{50}) and half-maximal cytotoxic concentration (CC_{50}) were calculated using the GraphPad Prism 9 software.

3. Results

3.1. Synthesis of derivatives with phenoxy group and aryl side chain

Candidate compounds with inhibitory effects on furin-like activity were designed using naturally occurring aromatic compounds modified with prenyl groups (Fig. 1). 2′,4′,6′-Trioxyacetophenone, orsellinic aldehyde, and umbelliferone were selected as the starting aromatic natural compounds. One equivalent of 3,3-dimethyl aryl bromide was introduced into each compound as an ether to yield prenyl derivatives (**C1**, **C3,** and **C5**). Derivatization focused on the presence of a hydroxy group and the length of the aryl side chain. Prenylation of 2′,4′-dioxyacetophenone yielded **C7**. Geranyl bromide was introduced instead of the 3,3-dimethyl aryl bromide-generated derivatives with longer side chains (**C2**, **C4**, **C6,** and **C8**). Considering the importance of the alkene in the prenyl unit, palladium in the carbon-catalyzed reduction of osthol generated the desired derivatives **C10** and ethyl ester **C9**. Fifteen derivatives, including the starting materials, were prepared for evaluation.

3.2. Evaluation of lead compounds for furin-like enzymatic activity inhibitors

The furin-like activity was evaluated using pyr-Arg-Arg-Ala-Arg-MCA as the fluorogenic substrate and cell lysates as whole proteolytic enzymes. Compounds **C1**, **C2, C3, C5, C8** and osthole inhibited furin-like activity (Fig. 2**A**). Among these 15 compounds, **C1** and **C2** were the most effective inhibitors of furin-like activity. Next, we evaluated whether these compounds had inhibitory effects on furin. To obtain furin, the secreted soluble furin (ssfurin) with a deleted transmembrane or cytoplasmic tail in the C-terminal region was expressed in HEK293 cells and purified (Fig. S2). Using furin as a fluorogenic substrate, we evaluated the inhibitory effects of furin on the 15 compounds (Fig. 2**B**). In the presence of 250 μM of compounds **C1**, **C2,** and osthole, furin

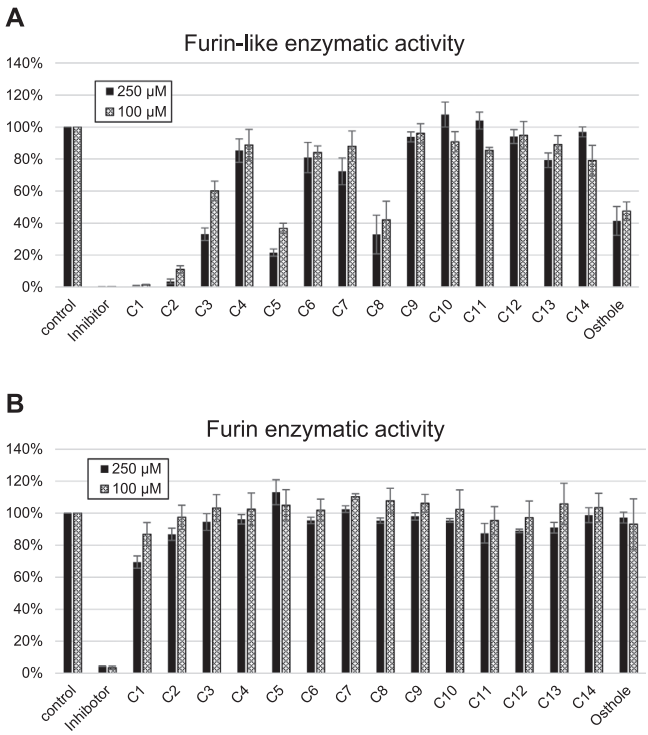

Fig. 2. The effects of compound C1–C14 and osthole on furin-like (A) and furin (B) activity based on fluorogenic substrates. Values represent the mean ± SD of three independent experiments (n = 3).

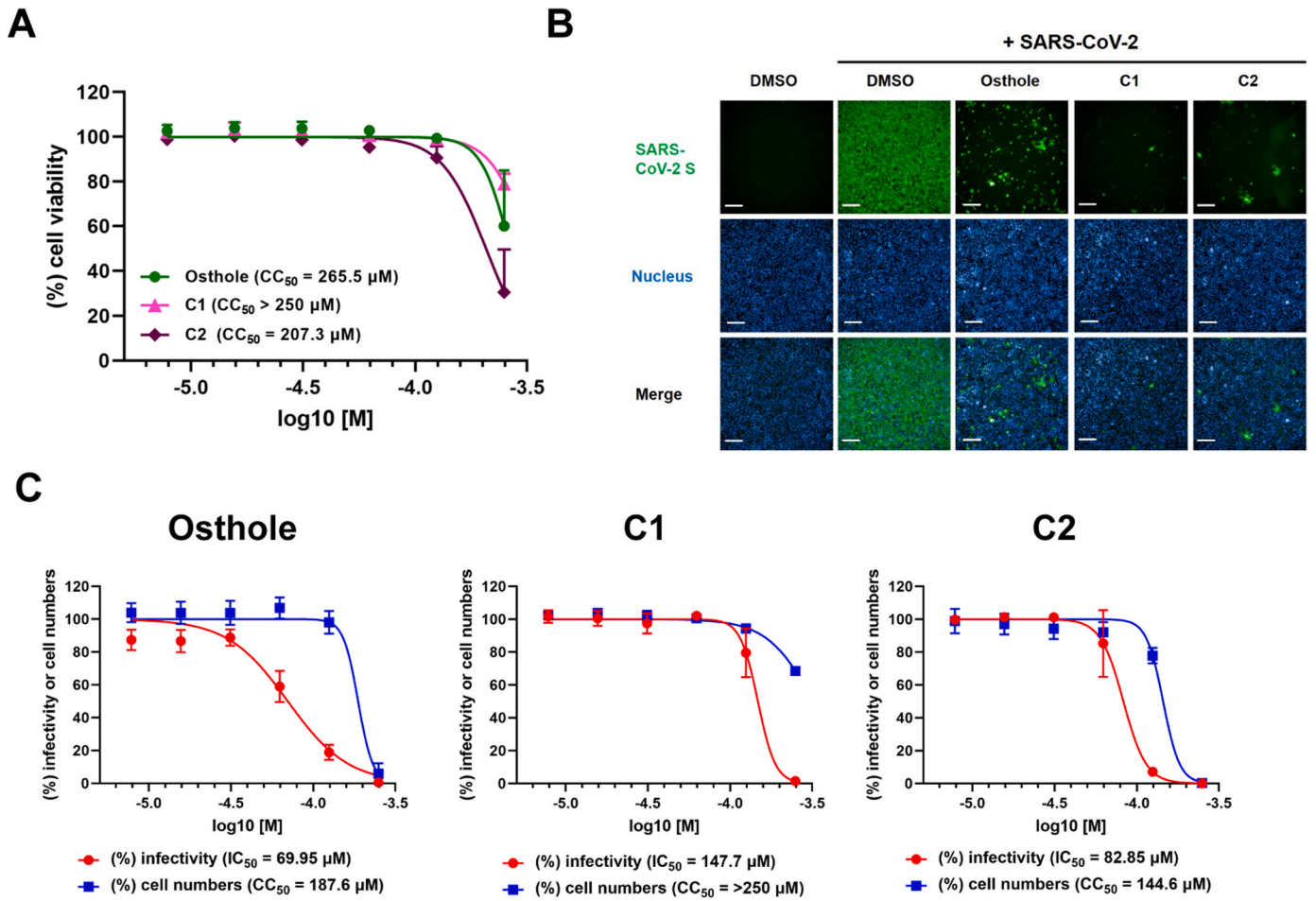

Fig. 3. The inhibitory effects of compound C1, C2 and osthole **on SARS-CoV-2 infection.** (A) Vero E6/TMPRSS2 cells were treated with osthole and compounds **C1** and **C2** at the indicated concentrations for 24 h. Cell viability was determined using CellTiter-Glo® Luminescent Cell Viability Assay. Results were normalized to those of dimethylsulfoxide (DMSO)-treated cells. (B) Vero E6/TMPRSS2 cells were infected with SARS-CoV-2 for 24 h at the indicated concentration of osthole and compounds **C1** and **C2.** The cells were then stained with anti-SARS-CoV-2 Spike RBD monoclonal antibody for viral infection and DAPI and analyzed to determine cell number and percent of infection. Representative fluorescence images show the SARS-CoV-2 S protein (green) and cell nucleus (blue). The concentrations of osthole and compounds **C1** and **C2** were 125 μM and 250 and 125 μM, respectively. Scale bar, 200 μm. (C) The percentages of infected cells and cell numbers were normalized to those of DMSO-treated cells infected with SARS-CoV-2. Values represent the mean ± SD of two independent experiments (n = 6).

activities were 69.5 ± 3.9%, 86.8 ± 3.8%, and 97.3 ± 3.4%, respectively. Compound **C1** had a slight inhibitory effect on furin activity, whereas other compounds, including compound **C2** and osthole, showed little inhibitory activity. To confirm the effects on furin-like and furin activities, we expressed a recombinant protein encoding the SARS-CoV-2 S1/S2 boundary sequence and evaluated the effects of FCS cleavage on furin-like and furin activities (Fig. S3). Compounds **C1**, **C2,** and osthole blocked S1/S2 cleavage through furin-like activities but not furin activities.

3.3. Evaluation of compounds for cellular antiviral potency

Focusing on osthole and compounds **C1** and **C2**, the inhibitory effects of SARS-CoV-2 infection in Vero E6/TMPRSS2 cells were evaluated. osthole and compound **C2** showed no cytotoxicity except for the highest concentration (125 μM). Compound **C1** showed no or minor cytotoxicity for all doses tested (Fig. 3**A**). In the infection study, we infected Vero E6/TMPRSS2 cells with SARS-CoV-2 in the presence of compounds **C1**, **C2,** and osthole at concentrations of 250, 125, 62.5, 31.25, 15.6, and 7.8 μM for 24 h followed by imaging analysis to calculate infectivity. All the three compounds suppressed SARS-CoV-2 infection in a dose-dependent manner. osthole and compound **C2** reduced viral replication by 41.1% and 14.7% at 62.5 μM and by 81.2% and 92.8% at 125 μM, respectively, with no cytotoxicity (Fig. 3**B and C**). Compound **C1** inhibited viral infection by 20.5% at 125 μM and by 98.5% at 250 μM with no or minor cytotoxicity (Fig. 3**B and C**). The IC_{50} values were 147.7, 82.85, and 69.95 μM for compounds **C1, C2,** and osthole, respectively.

4. Discussion

In this study, we synthesized and evaluated 15 compounds to determine their structure vs. property relationship on furin-like activity inhibition. **C1** and **C2** effectively inhibited the furin-like activity, whereas inhibition bt **C3**, **C5,** and **C8** was only mild. A comparison of these active compounds and their starting materials showed that aryl side chains were essential for inhibitory activity. The alkyl side chain without an alkene (**C10**) did not exhibit inhibitory activity, supporting the importance of the aryl unit. However, the number of hydroxy groups was the difference between the structures of the derivatives with significant furin-like activity (**C1** and **C2**) and the other derivatives. In **C1**, **C2**, **C3,** and **C8,** the hydroxy group at C-2 is chelated to a ketone or aldehyde. Additional hydroxy groups without chelation were present in **C1** and **C2,** which are important for increasing the activity.

In the present study, osthole showed inhibitory effects on furin-like activity but not on furin activity. Differences between furin-like and furin activities have been reported; the enzymatic activity of whole-cell

lysates expressing furin or knocked out with siRNA was not affected, suggesting that the furin-like activity of whole-cell lysates may be affected by other PCs [28]. Dicumanoyl compounds and coumarin dimers have been identified as noncompetitive furin inhibitors by screening a library of small molecules using enzyme-inhibitory assays with furin and fluorogenic substrates [29]. Coumarin has also been reported to show little inhibitory activity against furin, with an IC_{50} of less than 1 mM [29]. In this study, osthole, which has a coumarin skeleton, was ineffective against furin. Therefore, osthole's inhibition of furin-like activity may not be specific to furin but to other PCs or enzymes.

Lung tissues from COVID-19 patients showed syncytia, fused cells with multiple nuclei [30]. Tissue damage affects the disease severity and sequelae. Syncytia formation did not occur when the S protein mutated at the FCS site was transfected into Vero E6 cells or when furin/PC inhibitors were added to the cell medium[9]. Thus, the phenotypes of S protein activation by FCS cleavage, such as syncytia formation or SARS-CoV-2 cell entry, have been evaluated by mutating FCS to the S1/S2 boundary site or adding inhibitors to PCs. Enzymes involved in FCS cleavage were found to have furin-like enzymatic activity via furin/PCs. It has been reported that furin cells predominantly suppress the S protein of SARS-CoV-2 but do not abolish all its cleavage [31]. Cleaved S proteins were also observed in HEK293T cells in which Arg-X-X-Arg was replaced by a single Arg. Furin is thought to play a primary role in cleaving the FCS of the SARS-CoV-2 S protein. However, other PCs or enzymes that target a single-base residue may be responsible for FCS cleavage [31]. Further experiments using furin-deficient cells are required to investigate the inhibitory effects of **C1**, **C2,** and osthole on SARS-CoV-2 S protein cleavage.

Osthole is a multifunctional compound with anti-oxidative, anti-proliferative, anti-inflammatory, and anti-allergic properties [32] Osthole suppressed TGF-β1-induced epithelial-mesenchymal transition in lung cancer A549 cells[33]. Because TGF-β1 activates furin expression in several cell lines and proteolytic processing of the TGF-β1 precursor by furin is an essential step in the formation of biologically active TGF-β1, osthole may suppress TGF-β1-induced autocrine effects by blocking furin-like activities [34–36]. Furin activity is paramount to the viral infection cycle and could, therefore, be an attractive target for reducing the virulence of SARS-CoV-2. This inhibition may suppress infection two-fold by restricting viral entry into host cells and enhancing the immune response to promote viral clearance. Several protoxins and membrane fusion proteins of multiple viruses and bacteria, including the Ebola virus, Marburg virus, bird flu virus (H5N1), anthrax, and botulinum toxins, exploit host cell-surface PC processing for entry and infection [37]. Furin/PC antagonists may serve as useful prophylactic drugs against multiple furin-dependent pathogens. In conclusion, osthole, **C1**, and **C2**, which showed potent antiviral activity and no significant cytotoxicity, are promising lead compounds for developing anti-SARS-CoV-2 agents.

Funding

This work was partially supported by JSPS KAKENHI (grant numbers JP21K15283 and JP23K14372 to M.K., and JP22K06625 to T.H.).

CRediT authorship contribution statement

Hayashi Tsuyoshi: Conceptualization, Data curation, Funding acquisition, Investigation, Writing – original draft, Writing – review & editing. **Kamauchi Hitoshi:** Conceptualization, Data curation, Methodology, Writing – original draft. **Seki Taishi:** Data curation, Investigation. **Suzuki Ryuichiro:** Conceptualization, Investigation. **Kitamura Masashi:** Conceptualization, Data curation, Funding acquisition, Investigation, Methodology, Supervision, Writing – original draft, Writing – review & editing. **Kiba Yuka:** Data curation, Investigation. **Tanikawa Takashi:** Conceptualization, Methodology, Writing – original draft, Writing – review & editing.

Declaration of Competing Interest

The authors declare that they have no known competing financial interests or personal relationships that could have appeared to influence the work reported in this paper.

Data accessibility

The data supporting the findings of this study are available in the figures and supplementary materials.

Acknowledgment

Not applicable.

Authorship

TT, TH, HK, RS, and MK conceptualized and designed the study; YK, TT, TH, HK, TS, and MK acquired, analyzed, and interpreted the data; TT, TH, HK, and MK wrote the original draft; TT, TH, and MK supervised the study; TT gave final approval of the version to be submitted.

Appendix A. Supporting information

Supplementary data associated with this article can be found in the online version at doi:10.1016/j.biopha.2023.115940.

References

[1] P. Zhou, X.-L. Yang, X.-G. Wang, B. Hu, L. Zhang, W. Zhang, et al., A pneumonia outbreak associated with a new coronavirus of probable bat origin, Nature 579 (2020) 270, https://doi.org/10.1038/s41586-020-2012-7.
[2] C. Huang, Y. Wang, X. Li, L. Ren, J. Zhao, Y. Hu, et al., Clinical features of patients infected with 2019 novel coronavirus in Wuhan, China, Lancet 395 (2020) 497–506, https://doi.org/10.1016/S0140-6736(20)30183-5.
[3] WHO Coronavirus (COVID-19) Dashboard | WHO Coronavirus (COVID-19) Dashboard With Vaccination Data n.d. https://covid19.who.int/ (accessed April 27, 2023).
[4] COVID19 vaccine tracker n.d.
[5] I. Mohammed, A. Nauman, P. Paul, S. Ganesan, K.H. Chen, S.M.S. Jalil, et al., The efficacy and effectiveness of the COVID-19 vaccines in reducing infection, severity, hospitalization, and mortality: a systematic review, Hum. Vaccin Immunother. 18 (2022), https://doi.org/10.1080/21645515.2022.2027160.
[6] F. Wu, S. Zhao, B. Yu, Y.M. Chen, W. Wang, Z.G. Song, et al., A new coronavirus associated with human respiratory disease in China, 2020 579:7798, Nature 579 (2020) 265–269, https://doi.org/10.1038/s41586-020-2008-3.
[7] M. Hoffmann, H. Kleine-Weber, S. Schroeder, N. Krüger, T. Herrler, S. Erichsen, et al., SARS-CoV-2 cell entry depends on ACE2 and TMPRSS2 and is blocked by a clinically proven protease inhibitor, e8, Cell 181 (2020) 271–280, https://doi.org/10.1016/J.CELL.2020.02.052.
[8] J. Buchrieser, J. Dufloo, M. Hubert, B. Monel, D. Planas, M.M. Rajah, et al., Syncytia formation by SARS-CoV-2-infected cells, EMBO J. 39 (2020), https://doi.org/10.15252/EMBJ.2020106267.
[9] Y.W. Cheng, T.L. Chao, C.L. Li, M.F. Chiu, H.C. Kao, S.H. Wang, et al., Furin inhibitors block SARS-CoV-2 spike protein cleavage to suppress virus production and cytopathic effects, Cell Rep. 33 (2020), https://doi.org/10.1016/J.CELREP.2020.108254.
[10] Z. Xu, L. Shi, Y. Wang, J. Zhang, L. Huang, C. Zhang, et al., Pathological findings of COVID-19 associated with acute respiratory distress syndrome, Lancet Respir. Med 8 (2020) 420–422, https://doi.org/10.1016/S2213-2600(20)30076-X.
[11] R. Bussani, E. Schneider, L. Zentilin, C. Collesi, H. Ali, L. Braga, et al., Persistence of viral RNA, pneumocyte syncytia and thrombosis are hallmarks of advanced COVID-19 pathology, EBioMedicine 61 (2020), https://doi.org/10.1016/J.EBIOM.2020.103104.
[12] M. Hoffmann, H. Kleine-Weber, S. Pöhlmann, A multibasic cleavage site in the spike protein of SARS-CoV-2 is essential for infection of human lung cells, e5, Mol. Cell 78 (2020) 779–784, https://doi.org/10.1016/J.MOLCEL.2020.04.022.
[13] J. Shang, Y. Wan, C. Luo, G. Ye, Q. Geng, A. Auerbach, et al., Cell entry mechanisms of SARS-CoV-2, Proc. Natl. Acad. Sci. USA 117 (2020), https://doi.org/10.1073/PNAS.2003138117.
[14] E. Mehranzadeh, O. Crende, I. Badiola, P. Garcia-Gallastegi, What are the roles of proprotein convertases in the immune escape of tumors?, 2022, Vol 10, Page 3292, Biomedicines 10 (2022) 3292, https://doi.org/10.3390/BIOMEDICINES10123292.
[15] T. Horimoto, K. Nakayama, S.P. Smeekens, Y. Kawaoka, Proprotein-processing endoproteases PC6 and furin both activate hemagglutinin of virulent avian influenza viruses, J. Virol. 68 (1994) 6074–6078, https://doi.org/10.1128/JVI.68.9.6074-6078.1994.

[16] S. Hallenberger, V. Bosch, H. Angliker, E. Shaw, H.D. Klenk, W. Garten, Inhibition of furin-mediated cleavage activation of HIV-1 glycoprotein gp160. Nature 360 (1992) 358–361, https://doi.org/10.1038/360358A0.
[17] B.A. Johnson, X. Xie, A.L. Bailey, B. Kalveram, K.G. Lokugamage, A. Muruato, et al., Loss of furin cleavage site attenuates SARS-CoV-2 pathogenesis, Nature 591 (2021) 293, https://doi.org/10.1038/S41586-021-03237-4.
[18] T.P. Peacock, D.H. Goldhill, J. Zhou, L. Baillon, R. Frise, O.C. Swann, et al., The furin cleavage site in the SARS-CoV-2 spike protein is required for transmission in ferrets, 2021 6:7, Nat. Microbiol. 6 (2021) 899–909, https://doi.org/10.1038/s41564-021-00908-w.
[19] Y. Kiba, R. Oyama, S. Misawa, T. Tanikawa, M. Kitamura, R. Suzuki, Screening for inhibitory effects of crude drugs on furin-like enzymatic activities, J. Nat. Med 75 (2021) 1080–1085, https://doi.org/10.1007/S11418-021-01519-9/FIGURES/1.
[20] T. Tanikawa, T. Hayashi, R. Suzuki, M. Kitamura, Y. Inoue, Inhibitory effect of honokiol on furin-like activity and SARS-CoV-2 infection, J. Tradit. Complement Med 12 (2022) 69–72, https://doi.org/10.1016/J.JTCME.2021.09.005.
[21] P. Basabe, M. De Román, I.S. Marcos, D. Diez, A. Blanco, O. Bodero, et al., Prenylflavonoids and prenyl/alkyl-phloroacetophenones: synthesis and antitumour biological evaluation. Eur. J. Med Chem. 45 (2010) 4258–4269, https://doi.org/10.1016/J.EJMECH.2010.06.025.
[22] C.J. Chou, L.C. Lin, K.T. Chen, C.F. Chen, Novel acetophenones from fruits of evodia merrillii, J. Nat. Prod. 55 (1992) 795–799, https://doi.org/10.1021/NP50084A014.
[23] E.C. Row, S.A. Brown, A.V. Stachulski, M.S. Lennard, Design, synthesis and evaluation of furanocoumarin monomers as inhibitors of CYP3A4, Org. Biomol. Chem. 4 (2006) 1604–1610, https://doi.org/10.1039/B601096B.
[24] M.V.B. Reddy, C.R. Su, W.F. Chiou, Y.N. Liu, R.Y.H. Chen, K.F. Bastow, et al., Design, synthesis, and biological evaluation of Mannich bases of heterocyclic chalcone analogs as cytotoxic agents, Bioorg. Med Chem. 16 (2008) 7358–7370, https://doi.org/10.1016/J.BMC.2008.06.018.
[25] S. Genovese, F. Epifano, M. Curini, M. Dudra-Jastrzebska, J.J. Luszczki, Prenyloxyphenylpropanoids as a novel class of anticonvulsive agents, Bioorg. Med Chem. Lett. 19 (2009) 5419–5422, https://doi.org/10.1016/J.BMCL.2009.07.110.
[26] K. Hatsuzawa, M. Nagahama, S. Takahashi, K. Takada, K. Murakami, K. Nakayama, Purification and characterization of furin, a Kex2-like processing endoprotease, produced in Chinese hamster ovary cells, J. Biol. Chem. 267 (1992) 16094–16099, https://doi.org/10.1016/s0021-9258(18)41971-0.
[27] S. Matsuyama, N. Nao, K. Shirato, M. Kawase, S. Saito, I. Takayama, et al., Enhanced isolation of SARS-CoV-2 by TMPRSS2-expressing cells, Proc. Natl. Acad. Sci. USA 117 (2020) 7001–7003, https://doi.org/10.1073/PNAS.2002589117.
[28] G.L. Bourne, D.J. Grainger, Development and characterisation of an assay for furin activity, J. Immunol. Methods 364 (2011) 101–108, https://doi.org/10.1016/J.JIM.2010.11.008.
[29] T. Komiyama, J.M. Coppola, M.J. Larsen, M.E. van Dort, B.D. Ross, R. Day, et al., Inhibition of furin/proprotein convertase-catalyzed surface and intracellular processing by small molecules, J. Biol. Chem. 284 (2009) 15729–15738, https://doi.org/10.1074/JBC.M901540200.
[30] A. Saito, T. Irie, R. Suzuki, T. Maemura, H. Nasser, K. Uriu, et al., Enhanced fusogenicity and pathogenicity of SARS-CoV-2 Delta P681R mutation, Nature 602 (2022) 300–306, https://doi.org/10.1038/S41586-021-04266-9.
[31] G. Papa, D.L. Mallery, A. Albecka, L.G. Welch, J. Cattin-Ortolá, J. Luptak, et al., Furin cleavage of SARS-CoV-2 Spike promotes but is not essential for infection and cell-cell fusion, PLoS Pathog. 17 (2021), https://doi.org/10.1371/JOURNAL.PPAT.1009246.
[32] Y. Sun, A.W.H. Yang, G.B. Lenon, Phytochemistry, ethnopharmacology, pharmacokinetics and toxicology of cnidium monnieri (L.) cusson, Int J. Mol. Sci. 21 (2020), https://doi.org/10.3390/IJMS21031006.
[33] H. Feng, J.J. Lu, Y. Wang, L. Pei, X. Chen, Osthole inhibited TGF β-induced epithelial-mesenchymal transition (EMT) by suppressing NF-κB mediated Snail activation in lung cancer A549 cells, Cell Adh Migr. 11 (2017) 464–475, https://doi.org/10.1080/19336918.2016.1259058.
[34] M.J. O'Sullivan, J.A. Mitchel, C. Mwase, M. McGill, P. Kanki, J.A. Park, In well-differentiated primary human bronchial epithelial cells, TGF- β 1 and TGF- β 2 induce expression of furin, Am. J. Physiol. Lung Cell Mol. Physiol. 320 (2021) L246–L253, https://doi.org/10.1152/AJPLUNG.00423.2020.
[35] P. Stawowy, C. Margeta, H. Kallisch, N.G. Seidah, M. Chrétien, E. Fleck, et al., Regulation of matrix metalloproteinase MT1-MMP/MMP-2 in cardiac fibroblasts by TGF-beta1 involves furin-convertase. Cardiovasc Res 63 (2004) 87–97, https://doi.org/10.1016/J.CARDIORES.2004.03.010.
[36] C.M. Dubois, F. Blanchette, M.H. Laprise, R. Leduc, F. Grondin, N.G. Seidah, Evidence that furin is an authentic transforming growth factor-beta1-converting enzyme, Am. J. Pathol. 158 (2001) 305–316, https://doi.org/10.1016/S0002-9440(10)63970-3.
[37] W. Garten, Characterization of proprotein convertases and their involvement in virus propagation, Act. Virus Host Proteases (2018) 205, https://doi.org/10.1007/978-3-319-75474-1_9.